

# Gyrokinetic simulations of electrostatic microturbulence in ADITYA-U tokamak

Tajinder Singh<sup>1,\*</sup>, Deepti Sharma<sup>2</sup>, Tanmay Macwan<sup>2</sup>, Sarveshwar Sharma<sup>2,3,\*</sup>,  
Joydeep Ghosh<sup>2,3</sup>, Abhijit Sen<sup>2,3</sup>, Zhihong Lin<sup>4</sup>, Animesh Kuley<sup>1</sup>

<sup>1</sup>*Department of Physics, Indian Institute of Science, Bangalore 560012, India*

<sup>2</sup>*Institute for Plasma Research, Bhat, Gandhinagar 382428, India*

<sup>3</sup>*Homi Bhabha National Institute, Anushaktinagar, Mumbai, Maharashtra 400094, India*

<sup>4</sup>*Department of Physics and Astronomy, University of California Irvine, California 92697, USA*

*\*Emails: stjinder@iisc.ac.in, sarvesh@ipr.res.in*

## Abstract

A first-principles global gyrokinetic simulations of the electrostatic microturbulence driven by the pressure gradients of thermal ions and electrons are carried out for the ADITYA-U tokamak geometry using experimental plasma profiles with collisional effects. The dominant instability is determined to be trapped electron mode (TEM) based on the linear eigenmode structure and its propagation in the electron diamagnetic direction. The collisional effects suppress the turbulence and transport to a certain extent. The turbulent transport level of ion diffusivity determined by the nonlinear simulations is found to match well with the experimentally measured value of  $\sim 0.2 \text{ m}^2/\text{sec}$ . The electron heat diffusivity estimated from the experimentally measured energy confinement time is within 20% of the simulated value of  $\sim 1.2 \text{ m}^2/\text{sec}$ . Further nonlinear simulations by artificially suppressing the zonal flow show that the zonal flow is not playing any crucial role in the turbulence saturation, while the nonlinear saturation is dominated by the inverse cascade of the higher poloidal and toroidal modes to the lower one. The frequency spectrum of the electrostatic fluctuations, with broadband from  $\sim 0$  to 50 kHz, is also found to be in good agreement with the experimentally recorded spectrum in ADITYA-U.

## 1 Introduction

In fusion reactors [1, 2], the energy and particle confinement time must be long enough to achieve a net energy balance between the energy supplied to heat the system and the energy produced by the fusion process in the plasma. However, the energy and particle losses observed in magnetic fusion experiments are significantly higher than predicted values for the collisional processes [3]. This so-called anomalous transport is believed to be primarily due to small-scale instabilities called micro-instabilities caused by the temperature and density gradient of plasma species [4]. Therefore, understanding the physics of turbulent transport is of paramount importance in magnetically confined plasma experiments, as the balance between heat loss due to turbulent transport and self-heating by fusion products maintains ignition and hence controls the energy confinement time. The design of future reactors relies on the extrapolation of the turbulent transport levels from current fusion experiments to much larger future experiments such as the International Thermonuclear Experimental Reactor (ITER) [5, 6].

Thanks to the spectacular advances in high-performance computing, it has become possible to carry out large-scale numerical simulations, using various plasma models, to study the characteristics of turbulence and transport. For example, simulation results using sophisticated gyrokinetic codes [7] have shown excellent agreement with experimental observations from tokamaks. An important objective of these simulations is to find a physical basis for the empirical scaling of the turbulent transport levels from first-principles, state-of-the-art numerical modeling [8–10]. Advanced gyrokinetic simulation codes enable an in-depth study of small-scale turbulence, such as that arising from drift waves, that are widely believed to be the cause of anomalous transport [4]. Various simulation codes treat the problem at different levels of complexity to capture some of the crucial physics features, related to the small-scale modes like the ion temperature gradient (ITG) and the trapped electron mode (TEM).

Based on the numerical methods used to solve the underlying equations, the gyrokinetic codes are classified into three categories: Lagrangian, Eulerian and semi-Lagrangian. All these methods have their own advantages and disadvantages. The gyrokinetic codes such as GTC [11], ORB5 [12]

are based on the Lagrangian approach that represents the plasma by a finite number of marker particles. To reduce the particle noise due to Monte Carlo sampling of phase space these codes use the  $\delta f$  scheme [13]. The gyrokinetic codes GENE [14], GKV [15], GYRO [16] are based on the Eulerian approach. In this method, the time stationary phase space mesh is used for the discretization of the Vlasov equation. Whereas the semi-Lagrangian approach-based codes such as GYSELA [17] take the benefits of both the Lagrangian and Eulerian approaches with a good phase space description along with enhanced numerical stability.

Many gyrokinetic simulations of electrostatic microturbulence using realistic device geometry and experimental plasma profiles have witnessed the signatures of ITG/TEM turbulence. For example, a comparison of the experimentally measured plasma fluctuations and turbulent transport is made against the local electrostatic gyrokinetic simulations of L-mode discharge of DIII-D tokamak using the GS2 code [18], in which the ITG turbulence was investigated. The nonlinear electrostatic gyrokinetic simulations of L-mode discharge of DIII-D using the GYRO code show the similar electron temperature and density fluctuations in the ITG/TEM unstable plasma, consistent with the experimental observations [19]. Similarly, a validation study of the gyrokinetic electrostatic simulations using GYRO code has been done for the ITG and TEM dominated L-mode plasmas of Alcator C-Mod tokamak [20].

Gyrokinetic toroidal code (GTC) has also been applied to several different geometries, for example, tokamaks [21] and field-reversed configuration (FRC) [22] to study the turbulent transport. Recently, GTC is upgraded to simulate turbulences in the 3D devices called stellarators [23, 24]. In the present work, we have used GTC to study the microturbulence in ADITYA-U tokamak. ADITYA-U is a medium-sized, air-core tokamak, which has been recently upgraded from ADITYA tokamak [25–28] to incorporate a new set of divertor coils for shaped plasma operation with a new vacuum vessel along with a new toroidal belt limiter. Since its commissioning, several experiments relevant to the operation of future fusion devices such as ITER have been performed [26–28], including experiments on generation, transport and control of runaway electrons [27, 28], plasma disruption [27, 28], transient transport phenomena such as cold-pulse propagation [28, 29] and plasma detachment [28]. However, there are very few simulation studies on ADITYA-U tokamak and even the global simulation studies of the microturbulence by state-of-the-art codes like GTC are yet to be established.

In the present work, the self-consistent gyrokinetic simulations have been carried out using GTC to investigate the role of electrostatic microturbulence, such as ITG and TEM, in driving the turbulent transport in the circular plasmas (limiter plasmas) of ADITYA-U tokamak. The ion diffusivity and electron heat diffusivity values estimated from the experiments are in fair agreement with the values obtained from the simulations. The turbulent fluxes are found to be driven by the trapped electron mode (TEM) in ADITYA-U. The simulated spectra of electrostatic fluctuations match well with those measured using Langmuir probes in the edge region of the plasma. The simulations with and without collisions show that the collisional effects suppress the turbulence and transport to a certain extent. The nonlinear simulations by artificially suppressing the zonal flow shows that the zonal flow is not playing a crucial role in the turbulent transport, while the nonlinear saturation is dominated by the inverse cascade of the higher poloidal and toroidal modes to lower one. This study is the first step in understanding the turbulence and transport in ADITYA-U. These simulation findings could be helpful in setting up future experiments in ADITYA-U tokamak.

This paper is presented as follows: the geometry, equilibrium quantities, and experimental results for ADITYA-U tokamak discharge shot # 33536 are discussed in section 2. In section 3, the simulation and physics model used is presented. In section 4, linear and nonlinear simulations of the microturbulence are discussed. In section 5, the conclusions have been made.

## 2 ADITYA-U Experiment

ADITYA-U is a medium-sized tokamak with a major radius of 0.75 m and minor radius of 0.25 m [25–28]. For the present simulation, a hydrogen (main ion) plasma discharge (shot # 33536) has been used, in which the plasma is operated in the limiter configuration. The plasma parameters of the discharge are plasma current  $\sim 150$  kA, central chord-averaged density  $\sim 2.3 \times 10^{19} \text{ m}^{-3}$ , central chord-averaged electron temperature  $\sim 250$  eV and ion temperature  $\sim 80$  eV. The radial profile of plasma density has been obtained from a multi-channel microwave interferometer [29, 30].

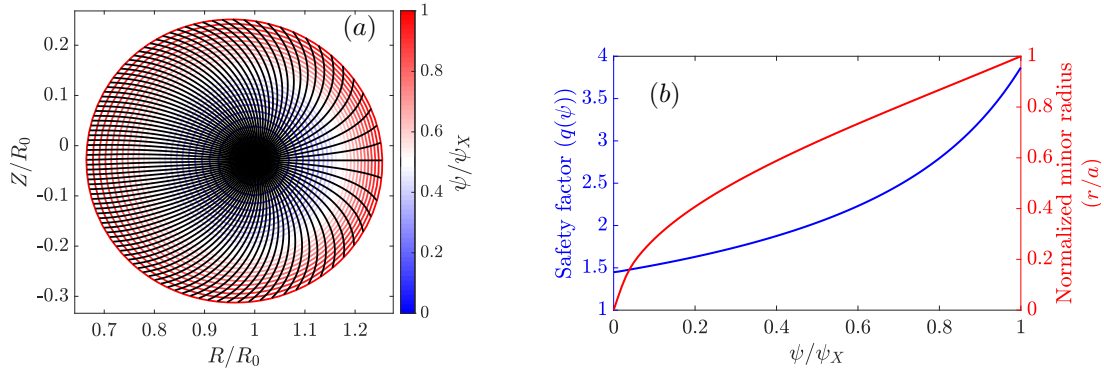


**Figure 1:** Equilibrium mesh on the poloidal plane (a). The contours show the poloidal flux normalized to the value at the last closed flux surface  $\psi_X$  and the black lines are the curves of constant poloidal angle and the safety factor (blue curve) and normalized minor radius (red curve) as a function of the normalized poloidal flux (b) for ADITYA-U discharge shot # 33536.

The radial profile of electron temperature is reconstructed using multi-chord soft X-ray emission intensity measurements in the core plasma region and Langmuir probe (single/triple) is used for the spectroscopic measurements of edge temperatures [29]. The core ion temperature is measured using spectroscopic diagnostics [31]. The radial profile of ion temperature is assumed to be the same as the plasma pressure profile. Figure 1a shows the equilibrium mesh on the poloidal plane for discharge shot # 33536 obtained with IPREQ code [32]. In the figure, the black lines show the curves of constant poloidal angle and contours show the poloidal flux normalized with the value at the last closed flux surface  $\psi_X$ . The on-axis magnetic field  $B_0$  is 1.44 T, the distance at the magnetic axis  $R_0$  is 0.7641 m. Figure 1b shows the safety factor profile obtained from the equilibrium simulations carried out using IPREQ code [32] and the normalized minor radius as a function of normalized poloidal flux. The equilibrium quantities for the ADITYA-U discharge are written in the cylindrical coordinates that are transformed to magnetic Boozer coordinates to be used as input to GTC. The edge region (region near to the last closed flux surface) of the ADITYA-U tokamak is thoroughly diagnosed by several sets of Langmuir probes [29]. A broadband fluctuation spectrum is observed in the frequency range of  $\sim 0$  to 50 kHz in the measured density fluctuations sampled at 100 kHz. The rack-Langmuir probes [29] are also used for the measurements of the radial profile of density in the edge regions. The particle diffusivity of  $\sim 0.2$  m<sup>2</sup>/sec in the edge region is derived from these measured density profiles [33], which are further cross-checked with UEDGE code simulations [34]. The energy confinement time is calculated by  $\tau_E = W/(P - dW/dt)$ , which is the ratio of stored energy to the input power (ohmic minus the power transferred to the plasma), that gives  $\tau_E \sim 10$  msec [33]. For microscopic diffusive processes, scaling of the energy confinement time with plasma size follows:  $\tau_E \sim a^2/4\chi_e$  [35], which gives  $\chi_e \sim 1.5$  m<sup>2</sup>/sec. The various ADITYA-U parameters and plasma parameters are shown in Table 1 for a typical experimental discharge.

### 3 Simulation and Physics Model

GTC uses the field-aligned coordinate system to study the magnetically confined plasma with nested flux surfaces [10] which is suitable for the efficient integration of particle trajectories that move primarily along the magnetic field lines. The fully kinetic dynamics of the plasma particles requires a smaller step size to resolve the cyclotron motion which in turn makes the simulations computationally expensive. To resolve this issue, a coordinate transformation is made from particle coordinates to the guiding-center coordinates. This transformation reduces the dimensionality of the system from 6D to 5D due to the averaging of the gyro-phase of the charged particles along the magnetic field lines [36, 37]. By doing so, the high-frequency cyclotron motion gets eliminated from the particle trajectory [38]. So, the resulting gyrokinetic equations involve the motion of the plasma particles in the reduced 5D space. The gyrokinetic equations describing the toroidal plasma in the

Minor radius	0.25 m
Major radius	0.75 m
On-axis magnetic field	1.44 T
On-axis electron temperature	250 eV
On-axis ion temperature	80 eV
On-axis electron density	$2.3 \times 10^{19} \text{ m}^{-3}$
Energy confinement time	$\sim 10$ msec
Ion acoustic speed	$1.55 \times 10^5$ m/sec
Ion gyro-radius	$6.34 \times 10^{-4}$ m
Electron gyro-radius	$2.61 \times 10^{-5}$ m
Ion thermal velocity	$8.76 \times 10^4$ m/sec
Electron thermal velocity	$6.63 \times 10^6$ m/sec

**Table 1:** ADITYA-U tokamak and plasma parameters for a typical experimental discharge.

inhomogeneous magnetic field in the five-dimensional space  $(\vec{X}, v_{\parallel}, \mu)$  is given by

$$\left( \partial_t + \dot{\vec{X}} \cdot \nabla + \dot{v}_{\parallel} \partial_{v_{\parallel}} \right) f_i(\vec{X}, \mu, v_{\parallel}, t) = C_i f_i, \quad (1)$$

$$\dot{\vec{X}} = v_{\parallel} \hat{b} + \vec{v}_E + \vec{v}_c + \vec{v}_g, \quad (2)$$

$$\dot{v}_{\parallel} = -\frac{\vec{B}^*}{m_i B} \cdot (\mu \nabla B + Z_i \nabla \phi), \quad (3)$$

where  $\vec{B}^* = \vec{B} + B v_{\parallel} / \Omega_i (\nabla \times \hat{b})$ ,  $C_i$  is the pitch-angle collision operator described in Ref. [39],  $\vec{v}_E$  is the  $\vec{E} \times \vec{B}$  drift velocity, and  $\vec{v}_c$ , and  $\vec{v}_g$  are magnetic drift velocities due to the curvature and gradient in magnetic field, that are given by

$$\vec{v}_E = \frac{c \hat{b} \times \nabla \phi}{B}, \quad (4)$$

$$\vec{v}_c = \frac{v_{\parallel}^2}{\Omega_i} \nabla \times \hat{b}, \quad (5)$$

$$\vec{v}_g = \frac{\mu}{m_i \Omega_i} \hat{b} \times \nabla B. \quad (6)$$

where  $B$  is the amplitude of equilibrium magnetic field at particle position,  $B^*$  is the equilibrium magnetic field amplitude at the guiding-center position of the particle,  $Z_i$  is the charge,  $m_i$  is the mass, and  $\Omega_i$  is the cyclotron frequency of the ion. To reduce the particle noise due to Monte Carlo sampling of the phase space,  $\delta f$  method [13] is used in which only the perturbed part of the particle distribution is evolved with time. The distribution function is written as the sum of equilibrium and perturbed parts,  $f_i = f_{0i} + \delta f_i$ , with the equilibrium part satisfying the 5D-gyrokinetic equation. Further, an additional dynamical variable, particle weight, is defined as  $w_i = \delta f_i / f_i$ , that satisfies the following equation

$$\frac{dw_i}{dt} = (1 - w_i) \left[ -\vec{v}_E \cdot \frac{\nabla f_{0i}}{f_{0i}} + \frac{Z_i \vec{B}^*}{m_i B} \cdot \nabla \phi \frac{1}{f_{0i}} \frac{\partial f_{0i}}{\partial v_{\parallel}} \right], \quad (7)$$

The electrostatic potential  $\phi$  appearing in particle equations of motion and weight equation is decomposed into a zonal component averaged over the flux surface and a fluctuating part  $\phi = \langle \phi \rangle + \delta \phi$  with  $\langle \delta \phi \rangle = 0$ , where  $\langle \dots \rangle$  represents the flux-surface averaging. To study the effect of electrons on turbulent transport and to comprise the instabilities like TEM in the simulations, the kinetic treatment of electrons is required. The kinetic treatment of electrons in the gyrokinetic framework requires a smaller time step due to fast parallel motion, thus increasing the simulation cost. To overcome this limitation, the fluid-kinetic hybrid model is implemented in GTC to study the turbulent transport due to the electrons [40]. In this model, to solve the drift kinetic equation for

electron, the electron response and electrostatic potential are expanded in the smallness parameter  $\delta$ , where  $\delta$  is the ratio of drift wave frequency to the electron transit frequency; as  $f_e = f_{0e} + \frac{e\delta\phi^{(0)}}{T_e}f_{0e} + \delta g_e$ , and  $\delta\phi = \delta\phi^{(0)} + \delta\phi^{(1)}$ . The nonadiabatic parts  $\delta g_e$ ,  $\delta\phi^{(1)}$  are smaller than the adiabatic parts by a factor of  $\delta$ . The electrostatic potential and electrostatic field involved in the gyrokinetic equations of the particles should be acquired from Poisson's equation in a spatial network of grids after the charge density is accumulated on the grids. However, in the gyrokinetic framework, gyrokinetic transformation needs to be incorporated in Poisson's equation as well. This results in a gyrokinetic version of Poisson's equation involving the electrostatic potential and particle density that are averaged over the charge ring with a radius of local gyro-radius of the charged particle. Numerically, this gyro-ring is represented by fewer points (4, 8, 16, etc). Usually, the four-point approximation is adequate to represent the gyro-ring. The non-zonal component of the electrostatic potential in the lowest order is acquired from the gyrokinetic Poisson equation given below

$$\frac{(\tau + 1)e\delta\phi^{(0)}}{T_e} - \frac{\tau e\delta\tilde{\phi}^{(0)}}{T_e} = \frac{\delta\bar{n}_i - \langle\delta\bar{n}_i\rangle}{n_0}, \quad (8)$$

where  $\tau = T_e/T_i$ ,  $n_0$  is the equilibrium electron density,  $\delta\tilde{\phi}^{(0)}$  is the second gyro-averaged perturbed potential defined as

$$\delta\tilde{\phi}^{(0)}(\vec{x}) = \frac{1}{2\pi} \int d^3\vec{v} \int d^3\vec{X} f_0(\vec{X}) \delta\bar{\phi}^{(0)}(\vec{X}) \delta(\vec{X} + \vec{\rho} - \vec{x}),$$

with  $\vec{x}$  and  $\vec{X}$  represents the coordinates of particle position and the particle guiding center position respectively and  $\vec{\rho}$  is gyro-radius vector.  $\delta\bar{\phi}^{(0)}$  is the first gyro-averaged perturbed potential defined by

$$\delta\bar{\phi}^{(0)}(\vec{X}) = \int d^3\vec{x} \int \frac{d\alpha}{2\pi} \delta\phi^{(0)}(\vec{x}) \delta(\vec{x} - \vec{X} - \vec{\rho}),$$

and similarly

$$\delta\bar{n}_i(\vec{x}) = \int d^3\vec{X} \int \frac{d\alpha}{2\pi} \delta f(\vec{X}) \delta(\vec{x} - \vec{X} - \vec{\rho}),$$

is the ion perturbed density at the guiding-center,  $\alpha$  is the gyro-phase. The second gyro-averaged perturbed electrostatic potential ( $\delta\tilde{\phi}^{(0)}$ ) is calculated using Padé approximation [41]. In the higher order, the electron dynamics is governed by the drift kinetic equation in  $\delta g_e$ . To resolve the electron dynamics, in a single push step for ion, electron is pushed several times, known as the subcyclotron ratio. An iterative time stepping sequence has been used to update the particle orbits and field quantities. At  $i$ th time step all the field quantities are computed and at  $(i + 1)$ th time step ion orbits are pushed using the ion gyrokinetic equation. The electron weight  $w_e = \delta g_e/f_e$  are evolved according to the equation

$$\frac{dw_e}{dt} = \left(1 - \frac{e\delta\phi^{(0)}}{T_e} - w_e\right) \left[ -\vec{v}_E \cdot \nabla \ln f_{0e}|_{v_\perp} - \frac{\partial}{\partial t} \left( \frac{e\delta\phi^{(0)}}{T_e} \right) - (\vec{v}_d + \delta\vec{v}_E) \cdot \nabla \left( \frac{e\phi}{T_e} \right) \right]. \quad (9)$$

where  $\delta\vec{v}_E = (c/B^*)\hat{b} \times \nabla\delta\phi$ , the notation ' $|_{v_\perp}$ ' indicates that the the gradient operator on ' $\ln f_{0e}$ ' is performed with  $v_\perp$  held fixed. The electron orbits are pushed from  $i$ th time step to  $(i + 1)$ th time step using all the field quantities at  $i$ th time step in Eq. (9). The non-zonal electrostatic perturbed potential till the first order correction is related to the density perturbation as

$$e^{e\delta\phi/T_e} = e^{e\delta\phi^{(0)}/T_e} - \frac{\delta n_e - \langle\delta n_e\rangle}{n_0}, \quad (10)$$

with  $\delta n_e = \int \delta h_e d^3\vec{v}$ . Equations (9) and (10) can be solved repeatedly to reach the higher order in the expansion. The convergence test shows that the second order expansion is sufficient for the present study. The equations for ions are solved only once. Finally, all the particle orbits and non-zonal components of field quantities are updated at  $(i + 1)$ th time step and the zonal component of the electrostatic potential at  $(i + 1)$ th time step is obtained by solving

$$\frac{\tau e \left( \langle\phi\rangle - \langle\tilde{\phi}\rangle \right)}{T_e} = \frac{\langle\delta\bar{n}_i\rangle - \langle\delta n_e\rangle}{n_0}. \quad (11)$$

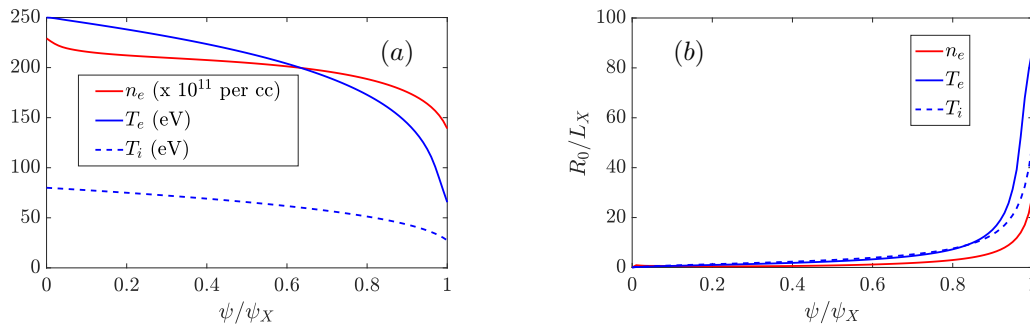


**Figure 2:** The profiles (a) and the corresponding normalized gradient (b) being used for the microturbulence simulations of ADITYA-U discharge shot # 33536.

The flux-surface-averaged gyrokinetic Poisson equation representing zonal component is solved by traditional integration, while a finite difference-based gyrokinetic Poisson solver is incorporated in GTC for the non-zonal component which uses the state-of-the-art HYPRE library [42] to solve the resulting matrix equation. The electrostatic field is then scattered back to the particle guiding-center position to update the particle orbit. The particles may encounter the simulation boundary during the push phase of the particle-in-cell cycle. The out-of-boundary particles are brought back to the simulation domain by the energy-conserving boundary conditions.

To take into account the neoclassical effects, Fokker-Planck collision operator for the collisions between like species and Lorentz pitch angle scattering operator for the collisions between unlike species, are implemented where the momentum and energy are enforced on the neoclassical mesh [39]. The dimensionless effective collision frequency defined in GTC is  $\nu^* = \epsilon^{-3/2} \nu q R_0 / v_{th}$ , with  $\epsilon = r/R_0$  as the local inverse aspect-ratio,  $r$  is the radius evaluated on the outer mid-plane,  $\nu$  is the physical collision frequency, and  $v_{th} = \sqrt{T_{0\alpha}/m_\alpha}$  is the thermal velocity of the plasma species  $\alpha$ .

## 4 Microturbulence Simulations

This work presents the electrostatic gyrokinetic simulations of the low-frequency drift wave instabilities driven by the gradient in the plasma density and temperature, performed using GTC. **The non-uniformities in the plasma profile acts as a source of free energy to excite the turbulence.** Figure 2 shows the plasma profile (2a) and the corresponding normalized gradient  $R_0/L_X$  (2b) used to run the **gradient-driven simulations**, where  $L_X$  is the profile gradient length scale given by  $1/L_X = -\partial(\ln X)/\partial r$ ,  $r$  is the local minor radius. The gradient in the plasma profile is steep at the last closed flux surface (LCFS) that can drive several electrostatic instabilities such as ion temperature gradient (ITG) instability, trapped electron mode (TEM) instability. The simulation domain is from  $\psi_{\text{inner}} = 0.1\psi_X$  to  $\psi_{\text{outer}} = 1.0\psi_X$ , where  $\psi$  values are normalized to the value at the last closed flux surface  $\psi_X$ . The ion species is proton and their dynamics is described by the gyrokinetic equations, and the electrons are treated kinetically, according to the fluid-kinetic hybrid model, as described in Sec. 2. The proton to electron mass ratio is taken as  $m_p/m_e = 1836$ . GTC uses three meshes: equilibrium mesh as shown in Fig. 1a, turbulence mesh, and neoclassical mesh. For the simulations, 200 radial grid points, 3000 poloidal grid points, and 32 grid points in the parallel direction are used. The microturbulences under investigation are ITG and TEM that satisfies  $k_{\parallel} \ll k_{\perp}$ , thus the turbulence mesh requires fewer grid points in the parallel direction as compared to the radial and poloidal grid points. The radial, poloidal and toroidal grid numbers used for the neoclassical mesh are 64, 64, 32, respectively, based on the convergence studies. First, the time step convergence is done, followed by the convergence of electron subcycles, and finally, the convergence for particle number is done. The time step size used is  $0.025R_0/C_s$ , where  $C_s/R_0$  is  $2.0258 \times 10^5 \text{ sec}^{-1}$  and  $C_s = \sqrt{T_e/m_i}$  is the ion-acoustic wave speed. The plasma is represented by the marker particles that are loaded uniformly throughout the simulation domain. From the convergence test, 50 marker particles per cell are used and the number of electron subcycles is kept 2. The system size in this work is set as  $a = 175\rho_i$ , where  $\rho_i$  is the ion gyro-radius.

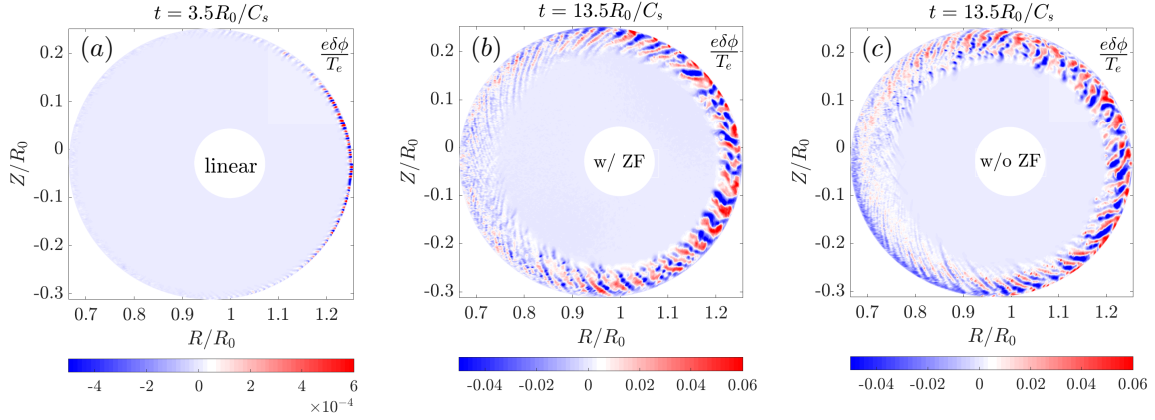


**Figure 3:** The electrostatic perturbed potential on the poloidal plane in the linear phase at time  $t = 3.5R_0/C_s$  (a), in the nonlinear phase at time  $t = 13.5R_0/C_s$  with zonal flow (b), and without zonal flow (c).

The effective charge number  $Z_{\text{eff}}$  is taken as 1.0 while considering the collisions in the simulations. The on-axis effective collision frequency  $\nu^*$  is 0.04 for electron and 0.26 for ion. The turbulent transport and the zonal flow physics are the universal aspects of the drift wave instabilities [4, 10]. To study the effect of zonal flow on the turbulent transport, an additional nonlinear simulation is run by artificially suppressing the zonal flow during the simulation. Figure 3 shows the poloidal cross-sections of the electrostatic perturbed potential at different simulation times of the two nonlinear simulations. Figure 3a shows the contour plot of the electrostatic potential in the linear phase of the simulation at time  $t = 3.5R_0/C_s$ . The linear eigenmode structure that peaks at the flux surface with  $\psi \sim \psi_X$  looks like a typical ballooning mode which is localized on the outer mid-plane side where the curvature is bad in the region of steep profile gradient with the eddies elongated along the direction of the profile gradient. On the flux surface, the mode structure is extended about the field lines and confined in the perpendicular direction. The mode propagates in the electron diamagnetic direction indicating that the TEM turbulence is unstable which is also consistent with the earlier gyrokinetic simulations of the DIII-D pedestal with steep profile gradients using GTC [21]. These findings are further supported by the earlier investigations made for the reversed field pinch (REP) [43], tokamak [44–49] and stellarator [50, 51] plasmas in the region of steep plasma profile gradients. Figures 3b and 3c show the contour plot of the electrostatic potential in the nonlinear phase of the simulation at time  $t = 13.5R_0/C_s$  with zonal flow (3b) and without zonal flow (3c). In the nonlinear phase due to the coupling between various toroidal and poloidal modes and the interaction with the self-generated zonal flow leads to the turbulence spreading from the edge to the core of the tokamak. It illustrates that the global effects play an important role in linking the turbulent transport from edge to the core of tokamak.

The radial-time variation of the root-mean-squared electrostatic potential has been shown in Fig. 4. Figure 4a shows the radial variation of root-mean-squared electrostatic potential at three different times  $t = 3R_0/C_s$  (blue),  $9R_0/C_s$  (red) and  $15R_0/C_s$  (black). It is clear that in the nonlinear stage turbulence structures spread far away from the location of linear eigenmode. The turbulence spreading takes place in the radial range  $\psi \in [0.68, 1.0]\psi_X$ . Figure 4b shows the time history of the root-mean-squared electrostatic potential in the region of turbulence spreading at three different flux surfaces with  $\psi = 0.80\psi_X$  (blue),  $0.90\psi_X$  (red), and  $0.98\psi_X$  (black). Thus, in the region of turbulence spreading TEM turbulence is unstable.

The role of zonal flow in regulating the turbulence is shown in Fig. 5, which shows the time history of root-mean-squared electrostatic potential without zonal flow (blue), with zonal flow (red) and the radial electric field resulting from the turbulence (black) at the flux surface with  $\psi = 0.98\psi_X$ . The blue and red lines are almost overlapping with each other, which shows that the zonal flow is not playing an important role in suppressing the turbulence rather the nonlinear saturation is dominated by the inverse cascade of the higher toroidal and poloidal modes to the lower one. Which is also clear from the comparison of Figs. 3b and 3c, as there is not much difference in the turbulence structure. These results are supported by the earlier findings by the local simulations, stating that

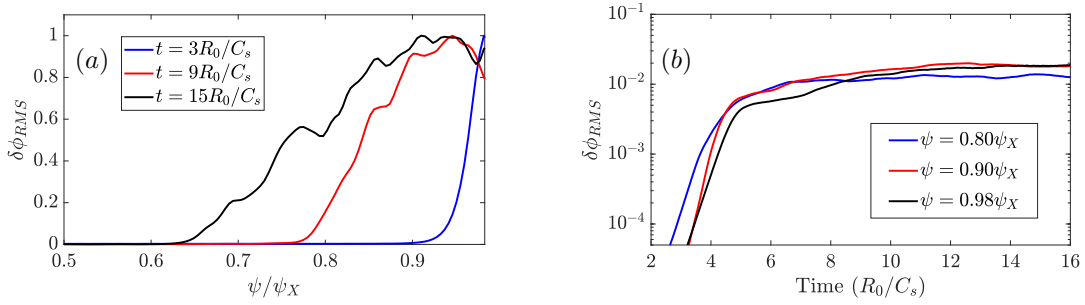


**Figure 4:** (a) The radial variation of the root-mean-squared electrostatic perturbed potential at three different times  $3R_0/C_s$  (blue),  $9R_0/C_s$  (red) and  $15R_0/C_s$  (black), and (b) the time history of the root-mean-squared perturbed electrostatic potential in the region of turbulence spreading at three different flux surfaces with  $0.80\psi_X$  (blue),  $0.90\psi_X$  (red), and  $0.98\psi_X$  (black).

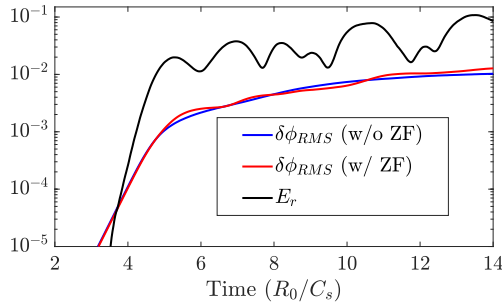


**Figure 5:** The time history of the root-mean-squared electrostatic perturbed potential without zonal flow (blue), with zonal flow (red) and the radial electric field resulting from the turbulence (black) at  $\psi = 0.98\psi_X$ .

the zonal flow has an important contribution to the turbulent transport driven by TEM instability only when  $\eta_e = \nabla \ln T_e / \nabla \ln n_e \lesssim 1$  [52] and for the current discharge of ADITYA-U,  $\eta_e \sim 4.0$  at  $\psi \sim \psi_X$ . Yet another global simulation study using GTC has shown that the zonal flow can play a crucial role in the case with  $T_e = T_i$  [53], while in ADITYA-U the electron temperature is about three times the ion temperature. Similarly, the flux-tube (local) simulations using GENE have shown that the zonal flow has little effect on the TEM turbulence saturation for the cases with strong electron temperature gradient and  $T_e = 3T_i$  [54], which is the case for ADITYA-U.

The dominant eigenmode is  $n = 73$ ,  $m = 271$  with the growth rate of  $\gamma = 2.98C_s/R_0$  and the real frequency of  $\omega = 2.79C_s/R_0$ . The wavenumber corresponding to the dominant mode is  $k_\perp \rho_i \sim 0.7$ . The simulations in the absence of collisions show that the collisions reduce the linear growth rate of the dominant mode by almost 9% and suppress the electrostatic fluctuations by almost 33%. The comparison of the root-mean-squared electrostatic potential without and with collisions is made in Fig. 6. Further, the collisions reduce the ion heat diffusivity by twice, the ion diffusivity by  $\sim 2.5$  times, the electron heat diffusivity by  $\sim 13\%$ , and the electron diffusivity by half. The effect of collisions on various quantities have been shown in Table 2. The root-mean-squared electrostatic potential and transport coefficients are averaged over times  $t \in [7.5, 15.0]R_0/C_s$ . Usually, the collisions have a stabilization effect on the TEM turbulence [55], but due to the smaller collision frequency for the trapped electrons than ions for the given gradients in the plasma profile, TEM turbulence remains unstable even in the presence of collisions. The TEM turbulence and transport suppression (to some extent) by the collisional effects is due to the de-trapping of electrons.

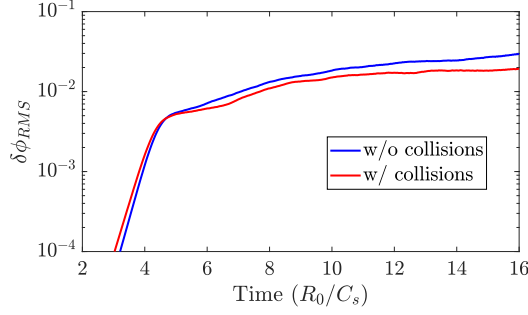


**Figure 6:** The time history of the root-mean-squared electrostatic perturbed potential without collisions (blue) and with collisions (red) at  $\psi = 0.98\psi_X$ .

	with collisions	without collisions
$\gamma$	2.98	3.24
$\delta\phi_{RMS}$	0.0152	0.0202
$D_i$	0.24	0.61
$D_e$	0.30	0.60
$\chi_i$	0.83	1.61
$\chi_e$	1.14	1.29

**Table 2:** The effect of collisions on the turbulence growth rate  $\gamma$  in units of  $C_s/R_0$ , the root-mean-squared electrostatic potential  $\delta\phi_{RMS}$  in units of  $T_e/e$  and the transport coefficients  $D_\alpha$ ,  $\chi_\alpha$  ( $\alpha = i, e$ ) in units of  $m^2/sec$ .

Figure 7 shows the 2D spectrum ( $|\delta\phi_{mn}|$ ) of the electrostatic perturbed potential on the flux surface with  $\psi = 0.98\psi_X$  in the linear phase at time  $t = 3.5R_0/C_s$  (7a) and in the nonlinear phase averaged over times  $t \in [7.5, 15.0]R_0/C_s$  (7b). Because of the ballooning feature of the microturbulence and the extension of the potential in the direction parallel to the magnetic field while confining in the perpendicular direction, the spectrum peaks on the mode rational surface (along the  $m = nq$  line) in the spectral domain. On the diagnosed flux surface  $\psi = 0.98\psi_X$ , the value of safety factor is  $q = 3.71$ . The spectrum in the linear phase is wide with a range  $n \in [40, 125]$ ,  $m \in [160, 460]$  with the most dominant mode at  $n = 73$ ,  $m = 271$ . The nonlinear coupling of the turbulent modes leads to the inverse cascade of the linearly unstable modes from high to low poloidal and toroidal modes. The spectrum in the nonlinear phase is averaged over the times  $t \in [7.5, 15.0]R_0/C_s$  that has a range  $n \in [0, 50]$ ,  $m \in [0, 190]$ .

The transport coefficients are calculated in GTC as

$$\chi_\alpha = \frac{1}{\langle |\nabla\psi|^2 \rangle n_{0\alpha} \frac{\partial T_{0\alpha}}{\partial\psi}} \left\langle \int d^3v \delta f_\alpha \left( \frac{1}{2} m_\alpha v^2 - \frac{3}{2} T_{0\alpha} \right) \vec{v}_E \cdot \nabla\psi \right\rangle$$

and

$$D_\alpha = \frac{1}{\langle |\nabla\psi|^2 \rangle \frac{\partial n_{0\alpha}}{\partial\psi}} \left\langle \int d^3v \delta f_\alpha \vec{v}_E \cdot \nabla\psi \right\rangle$$

where the angle bracket  $\langle \dots \rangle$  represents the flux-surface average and  $|\dots|$  represents the amplitude of the vector. GTC gives the diffusivity ( $D_\alpha$ ) and heat diffusivity ( $\chi_\alpha$ ) normalized by the Bohm values;  $D_B = \chi_B = cT_e/eB$ . The time history of the ion and electron diffusivities and heat diffusivities averaged over  $\psi \in [0.68, 1.0]\psi_X$  is shown in Fig. 8a. The transport coefficients first increase exponentially in the linear phase and then saturates in the nonlinear phase due to the mode coupling. Figure 8b shows the radial variation of the ion and electron diffusivities and ion heat diffusivities averaged over time  $t \in [7.5, 15.0]R_0/C_s$  at each radial grid point. The turbulence which is localized at  $\psi \sim \psi_X$  where the gradient in the profile is maximum, in the nonlinear phase spreads throughout the simulation domain due to the nonlinear mode coupling. **As there is not much**

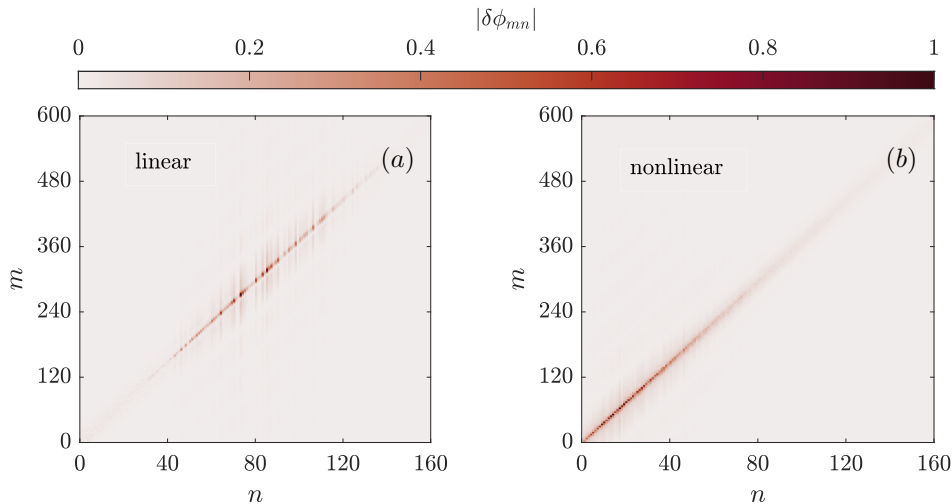


**Figure 7:** The 2D spectrum of the electrostatic potential on the flux surface  $\psi = 0.98\psi_X$  in the linear phase at time  $t = 3.5R_0/C_s$  (a) and in the nonlinear phase averaged over times  $t \in [7.5, 15.0]R_0/C_s$  (b).

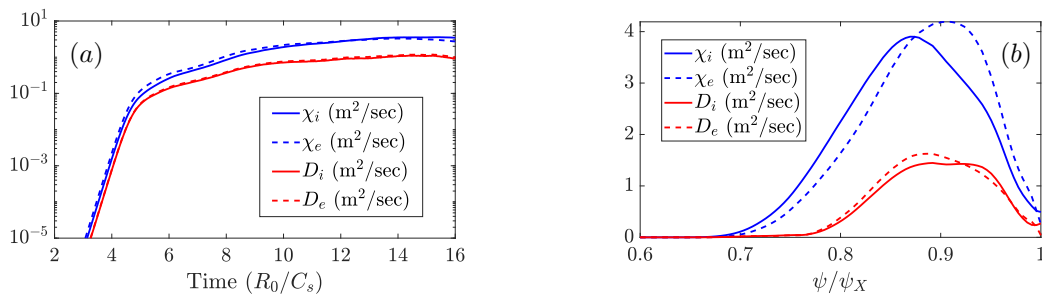


**Figure 8:** The time history (a) and radial variation (b) of the transport coefficients for ions and electrons.

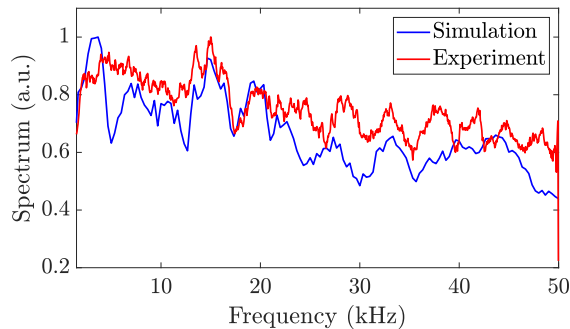
turbulence spreading near the magnetic axis, the central region  $\psi \in [0, 0.1]\psi_X$  has been excluded from the simulation domain.

Figure 9 shows the comparison of the spectrum of electrostatic fluctuations between experiment and simulation that spans from  $\sim 0$  kHz to 50 kHz, plotted on the outer mid-plane side of the flux surface with  $\psi = 0.98\psi_X$ . The experimentally recorded spectrum of electrostatic fluctuations shows a broadband of frequencies from  $\sim 0$  to 50 kHz (red) that matches well with the findings of the gyrokinetic simulations (blue) of ADITYA-U tokamak using GTC. The ion diffusivity near to the LCFS of tokamak predicted from the self-consistent simulations using GTC (see Fig. 8) is in good agreement with the value  $\sim 0.2$  m<sup>2</sup>/sec derived from the density profile [33], which is further cross-checked with UEDGE code simulations [34]. For the microscopic diffusive processes, the favorable scaling of energy confinement time with the plasma size suggests  $\chi_e \sim a^2/4\tau_E$ , where  $a$  is the minor radius (0.25 m) and  $\tau_E$  is the energy confinement time [35]. Experimentally,  $\tau_E$  is obtained by the usual method of dividing the stored energy by the power input (ohmic minus the power transferred to the plasma), that gives  $\tau_E \sim 10$  msec [33]. An estimate of the electron heat diffusivity obtained from the experiment is  $\chi_e \sim 1.5$  m<sup>2</sup>/sec, which is within 20% of the value  $\chi_e \sim 1.2$  m<sup>2</sup>/sec obtained from the simulations (see Fig. 8). Table 3 shows the comparison of the transport between the experiment and simulation near to the LCFS.

All these findings illustrate that the trapped electron mode (TEM) driven microturbulence is one of the dominant channels for driving the turbulent transport in ADITYA-U tokamak. These results may be important in setting up future ADITYA-U experiments.

(m <sup>2</sup> /sec)	Experiment	Simulation
$D_i$	0.2	0.24
$\chi_e$	1.5	1.20

**Table 3:** Comparison of the transport from experiment with the simulations near to LCFS.



**Figure 9:** The comparison of spectrum of the electrostatic fluctuations from simulation (blue) with experiment (red) near to the LCFS.

## 5 Conclusion and Discussion

To summarize, in this work, global gyrokinetic simulations of the electrostatic microturbulence in the ADITYA-U tokamak for shot # 33536 are carried out in the presence of collisions using gyrokinetic toroidal code (GTC). The linear eigenmode structure is dominated by a trapped electron driven instability, propagating in the electron diamagnetic direction with a real frequency of  $\sim 2.79C_s/R_0$ , and the growth rate of  $\sim 2.98C_s/R_0$ , that lies on the low wavenumber side with  $k_{\perp}\rho_i \sim 0.7$ . The simulations with and without collisions show that the collisional effects suppress the turbulence and transport to a certain extent. The nonlinear simulations of the microturbulence predict the ion diffusivity value, which agrees well with the experimentally measured value of  $\sim 0.2$  m<sup>2</sup>/sec. The electron heat diffusivity estimated from the experimentally measured energy confinement time is also within 20% of the simulated value  $\sim 1.2$  m<sup>2</sup>/sec. Further, the spectrum of electrostatic fluctuations shows broadband of frequencies from  $\sim 0$  to 50 kHz which also agrees with the spectrum obtained from the experiment. The nonlinear simulation by artificially suppressing the zonal flow shows that the zonal flow is not playing an important role in the turbulence saturation, while the nonlinear saturation is dominated by the inverse cascade of the high poloidal and toroidal modes to the lower one. These results are consistent with the previous studies [52–54]. Further, the global effects play an important role in linking the turbulence and transport from edge to the core of tokamak. Thus, the electrostatic microturbulence driven by the trapped electrons in the presence of collisions acts as one of the dominant channels for driving the anomalous turbulent transport in ADITYA-U tokamak. The current work is the first step to understand the turbulence and transport in ADITYA-U. From the experimental perspective, the insights gained from this electrostatic microturbulence study may be useful in setting up future ADITYA-U experiments. In the future, we plan to study the impurity transport by the electrostatic microturbulence in ADITYA-U.

## Acknowledgement

T.S. would like to thank J.H. Nicolau for the helpful discussion. The authors remain grateful to the ADITYA-U operation and diagnostic team for providing the data. This work is supported by National Supercomputing Mission (NSM) (Ref No: DST/NSM/R&D\_HPC\_Applications/2021/4), Board of Research in Nuclear Sciences (BRNS Sanctioned No. 39/14/05/2018-BRNS), Science and Engineering Research Board EMEQ program (SERB sanctioned no. EEQ/2017/000164) and Infosys Young Investigator award and US DOE SciDAC ISEP Center. A.S. is thankful to the Indian

1  
2  
3  
4 National Science Academy (INSA) for their support under the INSA Senior Scientist Fellowship  
5 scheme. The results presented in this work have been simulated on ANTYA cluster at Institute of  
6 Plasma Research, Gujarat, India, and SahasraT, Param Pravega supercomputers at Indian Institute  
7 of Science, Bangalore, India.  
8  
9

## 10 References

- 11 [1] J. Ongena, R. Koch, R. Wolf, and H. Zohm. Magnetic-confinement fusion. *Nature Physics*,  
12 12(5):398410, 2016.
- 13 [2] John Wesson and D. J. Campbell. *Tokamaks*. Oxford University Press, 2018.
- 14 [3] A.J. Wootton, B.A. Carreras, H. Matsumoto, K. McGuire, W.A. Peebles, Ch. P. Ritz, P.W.  
15 Terry, and S.J. Zweben. Fluctuations and anomalous transport in tokamaks. *Physics of Fluids*  
16 *B: Plasma Physics*, 2(12):2879–2903, 1990.
- 17 [4] W. Horton. Drift waves and transport. *Rev. Mod. Phys.*, 71:735–778, Apr 1999.
- 18 [5] B. Bigot. Progress toward ITER’s first plasma. 59(11):112001, Jun 2019.
- 19 [6] ITER: International Thermonuclear Experimental Reactor. <http://www.iter.org/>, 2021.
- 20 [7] J. Candy and R.E. Waltz. Anomalous transport scaling in the DIII-D tokamak matched by  
21 supercomputer simulation. *Phys. Rev. Lett.*, 91:045001, Jul 2003.
- 22 [8] Z. Lin, S. Ethier, T.S. Hahm, and W.M. Tang. Size scaling of turbulent transport in magneti-  
23 cally confined plasmas. *Phys. Rev. Lett.*, 88:195004, Apr 2002.
- 24 [9] W.M. Tang. Scientific and computational challenges of the fusion simulation project (FSP).  
25 *Journal of Physics: Conference Series*, 125:012047, Jul 2008.
- 26 [10] X. Garbet, Y. Idomura, L. Villard, and T.-H. Watanabe. Gyrokinetic simulations of turbulent  
27 transport. *Nuclear Fusion*, 50(4):043002, Mar 2010.
- 28 [11] Z. Lin, T.S. Hahm, W.W. Lee, W.M. Tang, and R.B. White. Turbulent transport reduction  
29 by zonal flows: Massively parallel simulations. *Science*, 281(5384):1835–1837, 1998.
- 30 [12] S. Jolliet, A. Bottino, P. Angelino, R. Hatzky, T.M. Tran, B.F. Mcmillan, O. Sauter, K. Appert,  
31 Y. Idomura, and L. Villard. A global collisionless PIC code in magnetic coordinates. *Computer*  
32 *Physics Communications*, 177(5):409–425, 2007.
- 33 [13] S.E. Parker and W.W. Lee. A fully nonlinear characteristic method for gyrokinetic simulation.  
34 *Physics of Fluids B: Plasma Physics*, 5(1):77–86, 1993.
- 35 [14] F. Jenko, W. Dorland, M. Kotschenreuther, and B.N. Rogers. Electron temperature gradient  
36 driven turbulence. *Physics of Plasmas*, 7(5):1904–1910, 2000.
- 37 [15] T.-H Watanabe and H. Sugama. Velocity–space structures of distribution function in toroidal  
38 ion temperature gradient turbulence. *Nuclear Fusion*, 46(1):24–32, Dec 2005.
- 39 [16] J. Candy and R.E. Waltz. An Eulerian gyrokinetic-Maxwell solver. *Journal of Computational*  
40 *Physics*, 186(2):545–581, 2003.
- 41 [17] V. Grandgirard, Y. Sarazin, P. Angelino, A. Bottino, N. Crouseilles, G. Darnet, G. Dif-  
42 Pradalier, X. Garbet, Ph. Ghendrih, S. Jolliet, G. Latu, E. Sonnendrücker, and L Villard.  
43 Global full-f gyrokinetic simulations of plasma turbulence. *Plasma Physics and Controlled*  
44 *Fusion*, 49(12B):B173–B182, Nov 2007.
- 45 [18] David W. Ross and William Dorland. Comparing simulation of plasma turbulence with exper-  
46 iment. II. Gyrokinetic simulations. *Physics of Plasmas*, 9(12):5031–5035, 2002.
- 47  
48  
49  
50  
51  
52  
53  
54  
55  
56  
57  
58  
59  
60

- 
- [19] A.E. White, L. Schmitz, G.R. McKee, C. Holland, W.A. Peebles, T.A. Carter, M.W. Shafer, M.E. Austin, K. H. Burrell, J. Candy, J.C. DeBoo, E.J. Doyle, M.A. Makowski, R. Prater, T.L. Rhodes, G.M. Staebler, G.R. Tynan, R.E. Waltz, and G. Wang. Measurements of core electron temperature and density fluctuations in DIII-D and comparison to nonlinear gyrokinetic simulations. *Physics of Plasmas*, 15(5):056116, 2008.
- [20] N.T. Howard, A.E. White, M.L. Reinke, M. Greenwald, C. Holland, J. Candy, and J.R. Walk. Validation of the gyrokinetic model in ITG and TEM dominated L-mode plasmas. *Nuclear Fusion*, 53(12):123011, Nov 2013.
- [21] D.P. Fulton, Z. Lin, I. Holod, and Y. Xiao. Microturbulence in DIII-D tokamak pedestal. I. Electrostatic Instabilities. *Physics of Plasmas*, 21(4):042110, 2014.
- [22] C.K. Lau, D.P. Fulton, I. Holod, Z. Lin, M. Binderbauer, T. Tajima, and L. Schmitz. Drift-wave stability in the field-reversed configuration. *Physics of Plasmas*, 24(8):082512, 2017.
- [23] H.Y. Wang, I. Holod, Z. Lin, J. Bao, J.Y. Fu, P.F. Liu, J.H. Nicolau, D. Spong, and Y. Xiao. Global gyrokinetic particle simulations of microturbulence in W7-X and LHD stellarators. *Physics of Plasmas*, 27(8):082305, 2020.
- [24] Tajinder Singh, Javier H. Nicolau, Zhihong Lin, Sarveshwar Sharma, Abhijit Sen, and Animesh Kuley. Global gyrokinetic simulations of electrostatic microturbulent transport using kinetic electrons in LHD stellarator. *Nuclear Fusion*, 2022.
- [25] R.L. Tanna, J. Ghosh, Harshita Raj, Rohit Kumar, Suman Aich, Vaibhav Ranjan, K.A. Jadeja, K.M. Patel, S.B. Bhatt, K. Sathyanarayana, P.K. Chattopadhyay, M.N. Makwana, K.S. Shah, C.N. Gupta, V.K. Panchal, Praveenlal Edappala, Bharat Arambhadiya, Minsha Shah, Vismay Raulji, M.B. Chowdhuri, S. Banerjee, R. Manchanda, D. Raju, P.K. Atery, Umesh Nagora, J. Raval, Y.S. Joisa, K. Tahiliani and S.K. Jha, and M.V. Gopalakrishna. Plasma production and preliminary results from the ADITYA upgrade tokamak. *Plasma Science and Technology*, 20(7):074002, May 2018.
- [26] R.L. Tanna, J. Ghosh, P.K. Chattopadhyay, Harshita Raj, Sharvil Patel, P. Dhyani, C.N. Gupta, K.A. Jadeja, K.M. Patel, S.B. Bhatt, V.K. Panchal, N.C. Patel, Chhaya Chavda, E.V. Praveenlal, K.S. Shah, M.N. Makawana, S.K. Jha, M.V. Gopalkrishana, K. Tahiliani, Deepak Sangwan, D. Raju, Umesh Nagora, S.K. Pathak, P.K. Atrey, S. Purohit, J. Raval, Y.S. Joisa, C.V.S. Rao, M.B. Chowdhuri, S. Banerjee, N. Ramaiya, R. Manchanda, J. Thomas, Ajai Kumar, Kumar Ajay, P.K. Sharma, S.V. Kulkarni, K. Sathyanarayana, B.K. Shukla, Amita Das, R. Jha, Y.C. Saxena, A. Sen, P.K. Kaw, and D. Bora and. Overview of recent experimental results from the Aditya tokamak. *Nuclear Fusion*, 57(10):102008, Jun 2017.
- [27] R.L. Tanna, Harshita Raj, J. Ghosh, Rohit Kumar, Suman Aich, Tanmay Macwan, D. Kumawat, K.A. Jadeja, K.M. Patel, M.B. Kalal, D.S. Varia, D.H. Sadharakiya, S.B. Bhatt, K. Sathyanarayana, B.K. Shukla, P.K. Chattopadhyay, M.N. Makawana, K.S. Shah, S. Gupta, V. Ranjan, V. Balakrishnan, C.N. Gupta, V.K. Panchal, Praveenlal Edappala, B. Arambhadiya, Minsha Shah, V. Raulji, M.B. Chowdhuri, S. Banerjee, R. Manchanda, G. Shukla, K. Shah, R. Dey, Nandini Yadava, Sharvil Patel, N. Bisai, D. Raju, P.K. Atrey, S.K. Pathak, U. Nagora, J. Raval, Y.S. Joisa, Manoj Kumar, K. Tahiliani, S.K. Jha, M.V. Gopalkrishana, and A. Sen. Overview of operation and experiments in the ADITYA-U tokamak. *Nuclear Fusion*, 59(11):112006, Jun 2019.
- [28] R.L. Tanna et al. Overview of recent experimental results from the ADITYA-U tokamak. *Nuclear Fusion*, page in print, 2021.
- [29] Tanmay Macwan, Harshita Raj, Kaushlender Singh, Suman Dolui, Sharvil Patel, Ankit Kumar, P. Gautam, J. Ghosh, R.L. Tanna, K.A. Jadeja, K.M. Patel, Rohit Kumar, Suman Aich, V.K. Panchal, Umesh Nagora, M.B. Chowdhuri, R. Manchanda, Nandini Yadava, Ritu Dey, Kiran Patel, J. Raval, S.K. Pathak, M.K. Gupta, K. Tahiliani, P.K. Chattopadhyay, A. Sen, Y.C. Saxena, R. Pal, and ADITYA-U Team. Gas-puff induced cold pulse propagation in ADITYA-U tokamak. *Nuclear Fusion*, 61(9):096029, Aug 2021.

- 
- [30] Praveen Kumar Atrey, Dhaval Pujara, Subroto Mukherjee, and Rakesh L. Tanna. Design, development, and operation of seven channels 100-GHz interferometer for plasma density measurement. *IEEE Transactions on Plasma Science*, 47(2):1316–1321, 2019.
- [31] G. Shukla, K. Shah, M.B. Chowdhuri, H. Raj, T. Macwan, R. Manchanda, U.C. Nagora, R.L. Tanna, K.A. Jadeja, K. Patel, K.B.K. Mayya, P.K. Atrey, and J. Ghosh and. Observations of toroidal plasma rotation reversal in the Aditya-U tokamak. *Nuclear Fusion*, 59(10):106049, Sep 2019.
- [32] Deepti Sharma, R. Srinivasan, Joydeep Ghosh, and P. Chattopadhyay. Aditya upgradation equilibrium study. *Fusion Engineering and Design*, 160:111933, 2020.
- [33] Tanmay Macwan. *Effect of Short Gas-puff Pulses and Biased-electrode on Transport, MHD Instabilities, Plasma-Wall Interaction and Runaway Electrons in ADITYA-U Tokamak*. PhD thesis, Homi Bhabha National Institute, 2022.
- [34] Ritu Dey et al. Simulations of edge plasma parameters of ADITYA-U tokamak using UEDGE code. to be submitted in *Nuclear Fusion*, 2021.
- [35] J.D. Callen and G.L. Jahns. Experimental measurement of electron heat diffusivity in a tokamak. *Phys. Rev. Lett.*, 38:491–494, Feb 1977.
- [36] Daniel H.E. Dubin, John A. Krommes, C. Oberman, and W.W. Lee. Nonlinear gyrokinetic equations. *The Physics of Fluids*, 26(12):3524–3535, 1983.
- [37] W.W. Lee. Gyrokinetic particle simulation model. *Journal of Computational Physics*, 72(1):243–269, 1987.
- [38] A.J. Brizard and T.S. Hahm. Foundations of nonlinear gyrokinetic theory. *Rev. Mod. Phys.*, 79:421–468, Apr 2007.
- [39] Z. Lin, W.M. Tang, and W.W. Lee. Gyrokinetic particle simulation of neoclassical transport. *Physics of Plasmas*, 2(8):2975–2988, 1995.
- [40] Z. Lin, Y. Nishimura, Y. Xiao, I. Holod, W.L. Zhang, and L. Chen. Global gyrokinetic particle simulations with kinetic electrons. *Plasma Physics and Controlled Fusion*, 49(12B):B163–B172, Nov 2007.
- [41] Yong Xiao, Ihor Holod, Zhixuan Wang, Zhihong Lin, and Taige Zhang. Gyrokinetic particle simulation of microturbulence for general magnetic geometry and experimental profiles. *Physics of Plasmas*, 22(2):022516, 2015.
- [42] Robert D. Falgout and Ulrike Meier Yang. Hypre: A library of high performance preconditioners. In Peter M.A. Sloot, Alfons G. Hoekstra, C.J. Kenneth Tan, and Jack J. Dongarra, editors, *Computational Science — ICCS 2002*, pages 632–641, Berlin, Heidelberg, 2002. Springer Berlin Heidelberg.
- [43] J.R. Duff, Z.R. Williams, D.L. Brower, B.E. Chapman, W.X. Ding, M.J. Pueschel, J.S. Sarff, and P.W. Terry. Observation of trapped-electron-mode microturbulence in reversed field pinch plasmas. *Physics of Plasmas*, 25(1):010701, 2018.
- [44] D.R. Ernst, P.T. Bonoli, P.J. Catto, W. Dorland, C.L. Fiore, R.S. Granetz, M. Greenwald, A.E. Hubbard, M. Porkolab, M.H. Redi, J.E. Rice, K. Zhurovich, and Alcator C-Mod Group. Role of trapped electron mode turbulence in internal transport barrier control in the Alcator C-Mod Tokamak. *Physics of Plasmas*, 11(5):2637–2648, 2004.
- [45] H. Arnichand, J. Citrin, S. Hacquin, R. Sabot, A. Krämer-Flecken, X. Garbet, C. Bourdelle, C. Bottureau, F. Clairet, J.C. Giacalone, Z.O. Guimarães-Filho, R. Guirlet, G. Hornung, A. Lebschy, P. Lotte, P. Maget, A. Medvedeva, D. Molina, V. Nikolaeva, and D. Prisiazhniuk. Identification of trapped electron modes in frequency fluctuation spectra. *Plasma Physics and Controlled Fusion*, 58(1):014037, Nov 2015.

- 
- 1  
2  
3  
4 [46] G.T. Hoang, C. Bourdelle, X. Garbet, G. Giruzzi, T. Aniel, M. Ottaviani, W. Horton, P. Zhu,  
5 and R.V. Budny. Experimental determination of critical threshold in electron transport on  
6 Tore Supra. *Phys. Rev. Lett.*, 87:125001, Sep 2001.  
7  
8 [47] J.C. Hillesheim, J.C. DeBoo, W.A. Peebles, T.A. Carter, G. Wang, T.L. Rhodes, L. Schmitz,  
9 G.R. McKee, Z. Yan, G.M. Staebler, K.H. Burrell, E.J. Doyle, C. Holland, C.C. Petty, S.P.  
10 Smith, A.E. White, and L. Zeng. Observation of a critical gradient threshold for electron  
11 temperature fluctuations in the DIII-D tokamak. *Phys. Rev. Lett.*, 110:045003, Jan 2013.  
12  
13 [48] D. Villegas, R. Guirlet, C. Bourdelle, G.T. Hoang, X. Garbet, and R. Sabot. Experimental  
14 electron temperature gradient dependence of heavy impurity transport in fusion devices. *Phys.*  
15 *Rev. Lett.*, 105:035002, Jul 2010.  
16  
17 [49] W.L. Zhong, X.L. Zou, C. Bourdelle, S.D. Song, J.F. Artaud, T. Aniel, and X.R. Duan. Con-  
18 vective velocity reversal caused by turbulence transition in tokamak plasma. *Phys. Rev. Lett.*,  
19 111:265001, Dec 2013.  
20  
21 [50] B.J. Faber, M.J. Pueschel, J.H.E. Proll, P. Xanthopoulos, P.W. Terry, C.C. Hegna, G.M. Weir,  
22 K.M. Likin, and J.N. Talmadge. Gyrokinetic studies of trapped electron mode turbulence in  
23 the helically symmetric experiment stellarator. *Physics of Plasmas*, 22(7):072305, 2015.  
24  
25 [51] C.B. Deng, D.L. Brower, D.T. Anderson, F.S.B. Anderson, A. Briesemeister, and K.M. Likin.  
26 Core density turbulence in the HSX stellarator. *Nuclear Fusion*, 55(12):123003, Oct 2015.  
27  
28 [52] D.R. Ernst, J. Lang, W.M. Nevins, M. Hoffman, Y. Chen, W. Dorland, and S. Parker. Role  
29 of zonal flows in trapped electron mode turbulence through nonlinear gyrokinetic particle and  
30 continuum simulation. *Physics of Plasmas*, 16(5):055906, 2009.  
31  
32 [53] Yong Xiao, Ihor Holod, Wenlu Zhang, Scott Klasky, and Zhihong Lin. Fluctuation character-  
33 istics and transport properties of collisionless trapped electron mode turbulence. *Physics of*  
34 *Plasmas*, 17(2):022302, 2010.  
35  
36 [54] Tilman Dannert and Frank Jenko. Gyrokinetic simulation of collisionless trapped-electron  
37 mode turbulence. *Physics of Plasmas*, 12(7):072309, 2005.  
38  
39 [55] F. Ryter, C. Angioni, A.G. Peeters, F. Leuterer, H.-U. Fahrbach, and W. Suttrop. Experi-  
40 mental study of trapped-electron-mode properties in tokamaks: Threshold and stabilization by  
41 collisions. *Phys. Rev. Lett.*, 95:085001, Aug 2005.  
42  
43  
44  
45  
46  
47  
48  
49  
50  
51  
52  
53  
54  
55  
56  
57  
58  
59  
60
-